analytical chemistry

pubs.acs.org/ac
Article

Automatic Blood Protein Enrichment by Magnetic-COF Polymers

Yuanyu Huang, T. Mamie Lih, Zhenyu Sun, Liyuan Jiao, Lijun Chen, and Hui Zhang*

Cite This: *Anal. Chem.* 2026, 98, 11261−11273
Read Online

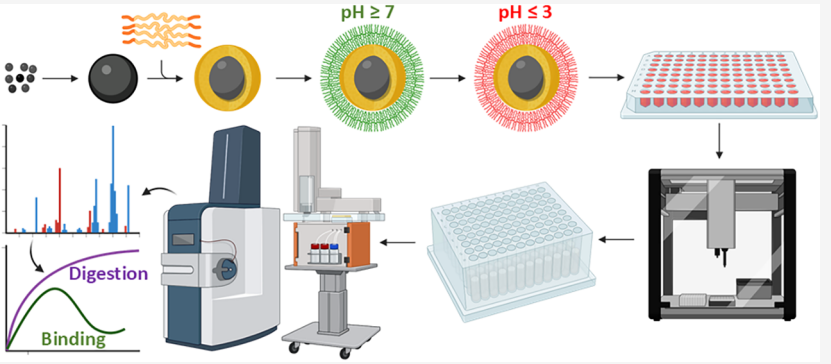

ABSTRACT: Blood proteome is a highly informative biological fluid, reflecting physiological and pathological states across the entire body. It contains thousands of proteins spanning a dynamic range of more than 10 orders of magnitude. This makes blood proteome an ideal matrix for disease diagnosis, prognosis, therapeutic selection, and monitoring. However, comprehensive and reproducible analysis of blood proteins remains technically challenging, primarily due to the overwhelming presence of high-abundance proteins that obscure low-abundance targets. Blood proteome analysis offers several advantages over tissue-based diagnostics: it enables real time, longitudinal sampling, captures systemic physiological or pathological changes, and provides access to tissue-derived proteins. Automation offers consistent handling, reduced human error, and better reproducibility, which are essential for translating proteomics into routine biomedical workflows. We designed this platform to integrate Magnetic-COF-based protein capture with scalable robotic handling, enabling blood protein enrichment and LC-MS/MS analysis, resulting in more than 4000 plasma proteins identified with a throughput of 30 samples per day. By combining molecular selectivity, magnetic enrichment, and automation, our strategy addresses key limitations in current blood proteomics workflows and offers a flexible foundation for the research and discovery of proteomics from pancreatic ductal adenocarcinoma patients.

INTRODUCTION

Blood proteome is an exceptionally informative biological matrix, reflecting the physiological and pathological states of the human body in real time.[1−4] It harbors thousands of proteins spanning over 10 orders of magnitude in concentration, encompassing a diverse repertoire of circulating factors, cellular secretions, and tissue leakage products.[5−7] This complexity renders blood an attractive source for disease diagnosis, prognosis, and therapeutic selection and monitoring.[7,8] However, the proteomics analysis of blood proteome remains technically challenging due to the dominance of high-abundance proteins, such as albumin and immunoglobulins,[9] which mask low-abundance disease-related proteins that are often of critical diagnostic and prognostic significance.[10,11] Pancreatic ductal adenocarcinoma (PDAC) is one of the leading causes of cancer-related death among different cancer types with low 5-year relative survival rates.[12] In 2025, 67,440 new cases and 51,980 deaths by PDAC were estimated in the United States.[13] PDAC is often diagnosed at a late stage, when upfront systemic therapy or resection is no longer feasible. Approximately 80 to 85% of patients present with either metastatic or unresectable disease.[14,15] This indicates that the early detection of PDAC may improve related surgery outcomes.[16] Emerging evidence suggests that the blood proteome can serve as a valuable reservoir for PDAC-specific proteins.[17,18] Circulating proteins derived from tumor cells, the tumor microenvironment, or systemic host responses can provide insights into disease stage, metastatic potential, drug resistance, and recurrence.[19−22] Moreover, blood analysis allows for real time, longitudinal monitoring of disease evolution and therapeutic efficacy—features that are crucial for precision oncology and adaptive treatment strategies.[23,24] Achieving deep proteomic coverage of plasma requires

Received: December 24, 2025
Revised: March 23, 2026
Accepted: March 24, 2026
Published: April 2, 2026

https://doi.org/10.1021/acs.analchem.5c08111
Anal. Chem. 2026, 98, 11261−11273

effective strategies to enrich low-abundance proteins while minimizing interference from high-abundance species.[25,26] In recent years, covalent organic frameworks (COFs) have emerged as promising materials for protein enrichment due to their customizable pore structures, large surface areas, and tunable chemical functionalities.[27−29] COFs are crystalline, porous polymers constructed from organic building blocks via strong covalent bonds, enabling precise control over their physical and chemical properties.[30,31] In our platform, we engineered Magnetic-COF by integrating superparamagnetic iron oxide nanoparticles (Fe_3O_4) with the COF backbone. This hybrid structure retains the selective adsorption capacity of COFs while allowing for rapid magnetic separation, which significantly enhances workflow efficiency. The porous architecture and surface chemistry of Magnetic-COF were optimized to facilitate the capture of diverse blood proteins, particularly those in the low-abundance range. Moreover, the magnetic properties enable automation-friendly handling, reducing processing time and manual variability.

We further integrated the Magnetic-COF with a liquid-handling robotic platform to achieve high-throughput and reproducible plasma proteome preparation. This system can fulfill the detection by LC-MS with 30 samples per day, with consistent identification of over 4000 plasma proteins, covering a wide dynamic range. The automation not only ensures standardized sample handling but also minimizes batch effects and improves intersample comparability—key factors for clinical translation. Its robustness and scalability make it ideally suited for large cohort studies aimed at blood protein discovery in PDAC. In this study, we present the development and validation of this automated Magnetic-COF-based platform and demonstrate its application in PDAC blood proteomic analysis. Our findings highlight the potential of this strategy to accelerate the integration of blood proteomics into clinical research and precision medicine.

To enable high-throughput and reproducible enrichment of blood proteins, we developed and automated a proteome enrichment workflow using high surface area magnetic covalent organic framework (Magnetic-COF) polymers. The protocol was executed on an Opentrons OT-2 liquid-handling robot using 96-well PCR plates. Each reaction used 100 μg of Magnetic-COF, with a total working volume of 180 μL per sample. The Magnetic-COF polymers used in this study were engineered to combine high surface area, shiftable porosity, and magnetic separability optimized for proteomic enrichment. To evaluate the proteomic depth afforded by Magnetic-COF enrichment, human blood samples were processed by using the automated protocol and analyzed by data-independent acquisition mass spectrometry (DIA-MS). Across technical replicates (n = 3), an average of 4,000 protein groups were identified per plasma sample. These data validated the robustness of the on-bead digestion approach in the automated platform and its applications in the proteomics analysis of 110 serum samples from pancreatic ductal adenocarcinoma patients with healthy controls.

METHODS

Synthesis of Magnetic Core and Magnetic-COF Polymers

In this study, the magnetic core Fe_3O_4 was first synthesized by the chemical coprecipitation method. Briefly, $FeCl_3{\cdot}6H_2O$ (10.8 g) and $FeCl_2{\cdot}4H_2O$ (3.9 g) were dissolved in distilled water (160 mL). After maintaining the temperature at 80 °C under the nitrogen atmosphere, 22 mL of ammonium hydroxide was added dropwise into the solution. The mixture was maintained at 80 °C for 1 h and then cooled to room temperature. The obtained black precipitates were washed with ethanol and water 3 times. 800 mg of black precipitates were suspended in 10 mL of 1,4-dioxane. Then, 320 mg of 2,5-Dimethoxybenzene-1,4-dicarbaldehyde (DMTA) was suspended in the mixture. After thorough mixing, 373 mg of 1,3,5-tri-(4-aminophenyl) benzene (TAPB) suspended in 10 mL of mesitylene was added to the mixture with mechanical stirring at 500 rpm. After mixing for 10 min, 3.3 mL of 3 M HOAc was added dropwise to the mixture. Then, the mixture was reacted at 25 °C for 72 h. Afterward, a dark yellow precipitate was obtained, which was then separated by a magnetic and washed by ethanol, methanol, and water 3 times each. Finally, the obtained Magnetic-COF polymers were suspended in methanol.

Characterization Tools

The morphology and elemental analysis of the Fe_3O_4 cores and Magnetic-COF polymers were characterized by using transmission electron microscopy (Hitachi 7600 TEM) at an operating voltage of 80.0 kV. Images were acquired by a Dual AMT CCD camera system with XR80 high-resolution high-speed (8 M pixel, 16-bit) camera. The distribution of particle size and zeta potential of the Magnetic-COF polymers were measured using a Zetasizer Pro (Malvern) at 25 °C in water.

Biological Fluids Samples

The human plasma, serum, and whole blood samples used as a control for the automatic platform optimization were purchased from Innovative Research. Serum specimens from patients with PDAC were obtained from the University of Calgary GI/HPB Tumor Bank under approval from the Health Research Ethics Board of Alberta (HREBA.CC-16−0769).[14] Written informed consent was obtained from all participants. Blood was collected prior to surgical intervention for pancreatic masses using gold-topped vacutainer tubes (BD Biosciences) containing a clot activator and a gel separator. Within 6 h of collection, samples were centrifuged and the resulting sera were stored at −20 °C until shipment. A total of 110 human serum samples (55 PDAC and 55 nondiseased controls) were shipped to Johns Hopkins University for mass spectrometry−based proteomics analyses. Control samples were matched to PDAC cases by age and sex. All specimens were deidentified before transfer to ensure confidentiality. Detailed procedures for specimen collection and processing are available in the previously published study.[16] The 110 PDAC serum samples were randomly assigned to two 96-well plates and analyzed across two independent LC−MS/MS batches (Supporting Tables).

Sample Processing by Automatic Enrichment, Lysis, and Digestion

In this study, 125 μL of blood samples were collected into the 96-well PCR plate as the preparation step for the enrichment. A total of 100 μg of Magnetic-COF beads were suspended by ultrasonication for 5 min and transferred into another 96-well PCR plate with matched positions to biological fluid samples, followed by adding 180 μL of solvent (0.1% formic acid (FA, Sigma)) to each well of Magnetic-COF beads. After mixing by pipet mixing, the washing solvent was removed by the magnetic module. For the enrichment process, 100 μg of Magnetic-COF beads were suspended by 50 μL of 0.1% FA and mixed with 125 μL of blood samples. The total 175 μL of mixture was incubated at room temperature for 30 min at 1600 rpm. High-abundant proteins were removed by 5 rounds of washing steps with 180 μL of 0.1% FA after mixing for 1 min at 1,600 rpm each. In each well, Magnetic-COF beads with enriched proteins were lysed by 40 μL of 8 M urea and reduced with 10 μL of 100 mM dithiothreitol (DTT) for 10 mM final concentration. Then the lysis step was processed at room temperature for 60 min at 1600 rpm, followed by alkylation with 10 μL of 100 mM iodoacetamide (IAA) with a final concentration of 20 mM at room temperature for 25 min at 1600 rpm in the dark. Then the mixture in each well was digested with 1 mAU of Lys-C (Wako Chemicals) at 37 °C for 60 min at 1600 rpm, then diluted with 100 μL of 50 mM Tris-HCl (pH 8.0) and digested with

https://doi.org/10.1021/acs.analchem.5c08111
Anal. Chem. 2026, 98, 11261−11273

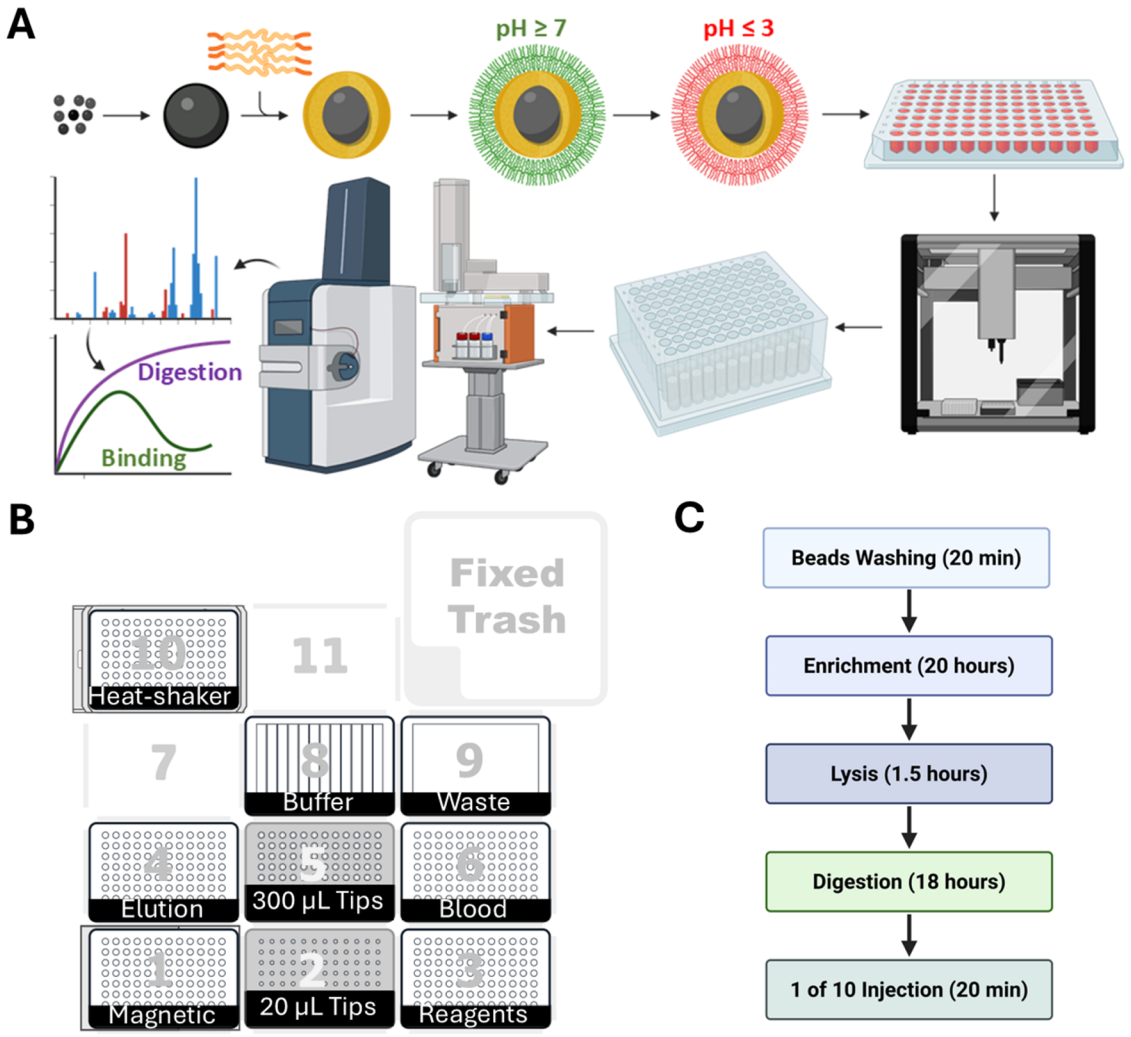

Figure 1. Automated Magnetic-COF–based blood proteomics workflow. (A) Schematic illustration of the Magnetic-COF polymers design and enrichment processes. (B) Labware layout for automated sample preparation on the robotic liquid-handling platform. (C) Schematic overview of the main steps with estimated time consuming in the automated workflow.

2.5 μg of sequencing-grade modified trypsin (Promega) at 37 °C for 16 h at 1600 rpm. The digested samples were then acidified with 10 μL of 40% FA to the pH value less than 3.0, in which Magnetic-COF were shown as dark red beads. All digested samples were directly injected into Evo-tips with 1 of 10 injections, along with small-molecule impurities such as Tris-HCI and urea removed.

LC-MS/MS Analysis

All of the LC-MS/MS data were acquired in DIA mode via an Evosep One EV-1000 (EVOSEP) system coupled with a timsTOF HT (Bruker) mass spectrometer. The 15 cm × 150 μm PepSep C18 column (1.5 μm, Bruker) was used for peptide separation with a 44 min gradient length. The LC gradient was from 3 to 35% of the B phase at 50 °C with a flow rate of 0.5 μL/min. The detection throughput was annotated as "30 SPD" (30 samples per day). The MS1 scan range of 100–1700 m/z and MS2 scan range of 338.6–1338.6 m/z were acquired under the dia-PASEF mode. 1/K0 was ranged from 0.70 to 1.45 V/s/cm^2 with the Ramp time equal to 85 ms.

Data Processing and Analysis

All the raw files were searched against a UniProt/Swiss-Prot database containing reviewed proteins from *Homo sapiens* (downloaded on 2023/09, 20,426 entries) using the directDIA approach in the Spectronaut (version 18.5, Biognosys). Dynamic with a correction factor of 1 was set as the mass tolerance of MS and MS/MS. Precursors were filtered by the cutoff of 0.01 of the Q value, also annotated as the FDR cutoff at 1%. Carbamidomethyl (C) was set as a fixed modification. Acetyl (Protein N-term) and Oxidation (M) were set as variable modifications. The quantification of a protein was calculated by the sum of its top 3 stripped sequences with their quantity results.

Reproducibility among the triplicates was determined based on the Spearman correlation. Differential analysis was carried out by calculating the median log 2-fold changes between cancer and control groups, and differential proteins were defined using two-sided t tests with Benjamini–Hochberg correction (FDR < 0.05) and an absolute $\log_2$ fold-change ≥ 1. The two-sided t test was performed with the p-value adjusted via the Benjamini–Hochberg method.

RESULTS AND DISCUSSIONS

Automatic Magnetic-COF Enrichment Workflow and LC-MS/MS Analysis

In this study, we developed an automated workflow that integrates Magnetic-COF enrichment with robotic handling and DIA-MS analysis (Figure 1A). The workflow consists of magnetic capture, washing, on-bead tryptic digestion, peptide elution, and mass spectrometric acquisition. The incorporation of an Opentrons OT-2 liquid-handling system enables reproducible, high-throughput sample preparation that pro-

https://doi.org/10.1021/acs.analchem.5c08111
Anal. Chem. 2026, 98, 11261–11273

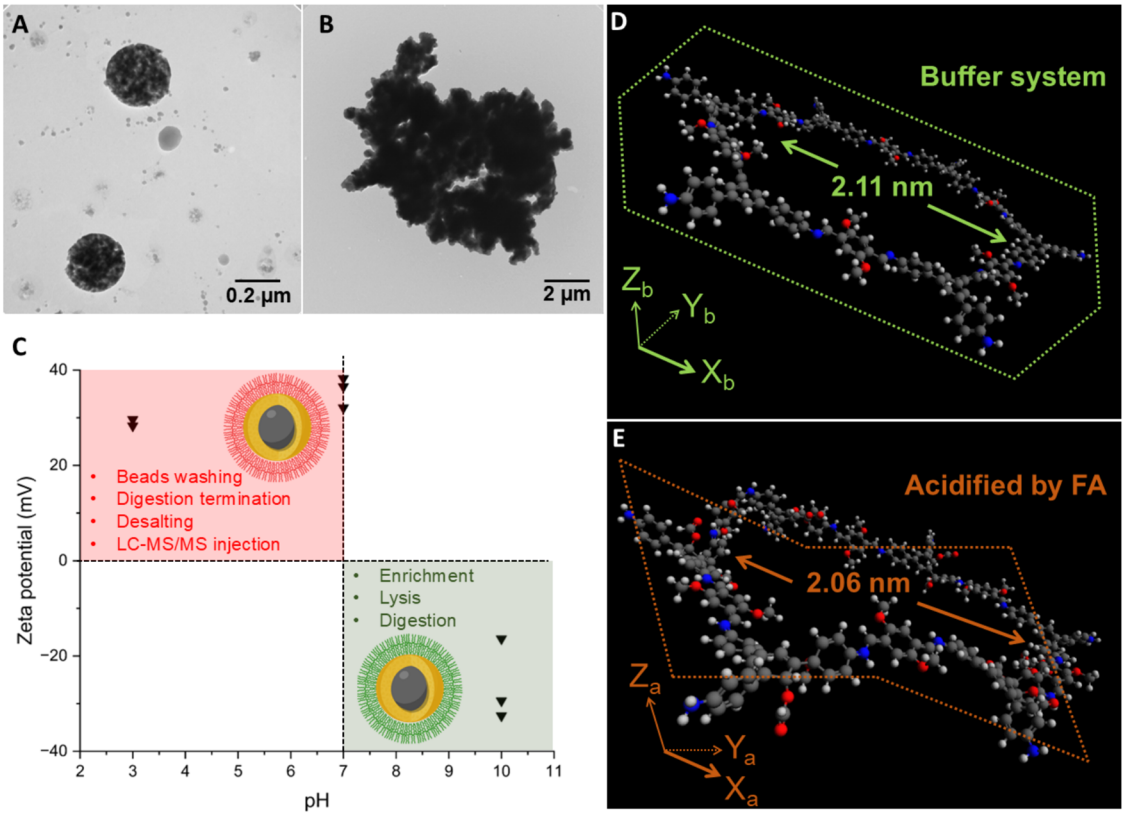

Figure 2. Structural and physicochemical characterization of Magnetic-COF polymers. (A) TEM image of the magnetic Fe_3O_4 nanoparticle core. (B) TEM image of the Fe_3O_4@COFs hybrid showing the core−shell Magnetic-COF architecture. (C) Zeta potential measurements of Magnetic-COF in suspension at pH 3.0, 7.0, and 10.0. (D) Pore structure of Magnetic-COF in buffer and (E) upon acidification with formic acid, optimized geometry demonstrated by Avogadro v1.2.0. Carbon, hydrogen, oxygen, and nitrogen atoms were labeled with gray, white, red, and blue spheres, respectively.

cesses up to 96 samples in 48 h with minimized manual variation and efficient labware layout (Figure 1B,C). This integrated platform addresses bottlenecks of scalability and reproducibility in plasma, serum, and whole blood proteomics, allowing steady identification of more than 4000 plasma proteins per sample at a throughput of 30 samples per day with an enzyme digestion time curve and saturation binding curve described for the optimization processes.

Characterization of Magnetic-COF Polymers

The physicochemical properties of Magnetic-COF were examined to establish their suitability for blood protein enrichment. TEM images revealed uniform Fe_3O_4 cores with the size of around 300 nm (Figure 2A) and the successful formation of a core−shell-based sheet architecture after the assembly of COF (Figure 2B). Particle size distribution analysis by dynamic light scattering (DLS) shows that the Magnetic-COF form micrometer-scale polymers with a defined size distribution around 1.26 μm optimized for efficient magnetic separation and automatic handling (Figure S1). Zeta potential analysis confirmed surface charge characteristics affected by the pH in the suspension of Magnetic-COF polymers (Figure 2C), while pore structure modeling demonstrated a stable 2-D porous framework in the buffer system at 2.11 nm inner diameter on average (pH 8.0, Figure 2D) and altered 3-D porous geometry under acidification by formic acid that decreased the average inner diameter to 2.06 nm due to the change of orbital hybridization at pore vertexes (pH 3.0, Figure 2E). This pore structure shift was verified to be reversible by the repeated adjustment of the pH in the suspension of Magnetic-COF polymers (Figure S2). These observations confirm both the structural integrity and environmental responsiveness of Magnetic-COF, which are crucial for selective protein capture and compatibility with diverse sample preparation conditions. Changes in solvent composition and pH induce modest but reversible pore-size adjustments that regulate surface accessibility. Under acidic conditions (0.1% formic acid), pore contraction facilitates the removal of residual contaminants and widely binding proteins, regenerating accessible binding sites. Upon transition to neutral or near-neutral pH conditions during protein binding, lysis, and on-bead digestion, pore expansion increases surface accessibility, promoting adsorption of proteins and binding of peptides. Final acidification during digestion termination induces pore contraction, facilitating the peptide elution step. The selective enrichment effect arises from the combined contributions of pH-dependent zeta potential, hydrogen bonding, and $\pi-\pi$ interactions from the aromatic COF backbone, together with differential adsorption and desorption processes during repeated washing steps, which collectively ensure the selective protein enrichment toward reproducible blood proteomics.

Optimizations of Plasma Proteomics

The enrichment performance of the automated platform was validated by time-course and binding capacity analysis. Missed cleavage rates decreased steadily with longer digestion times, paralleled by consistent numbers of plasma proteins identified

https://doi.org/10.1021/acs.analchem.5c08111
Anal. Chem. 2026, 98, 11261−11273

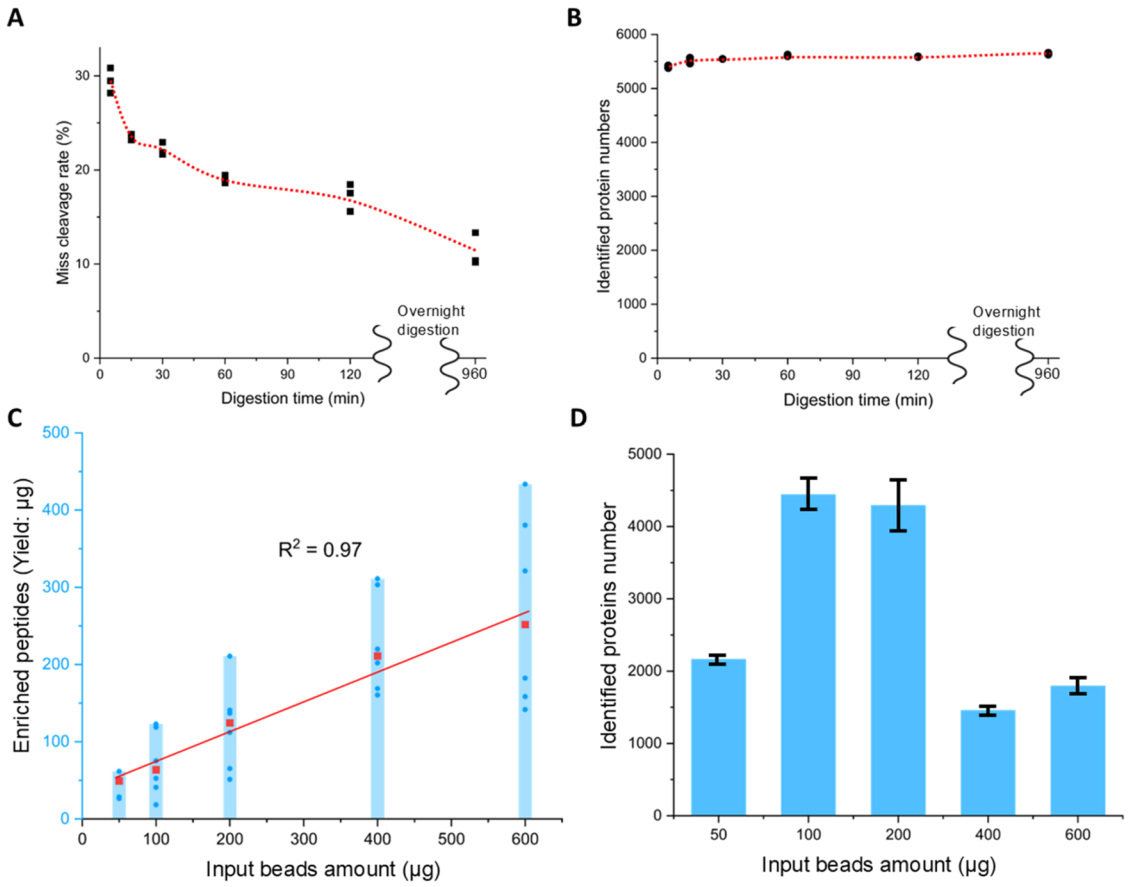

Figure 3. Optimization of blood protein enrichment by Magnetic-COF. Trypsin digestion time curves of automatic plasma proteome enrichment by Magnetic-COF polymers characterized by (A) miss cleavage rate and (B) total quantitation results. Saturation binding curves of automatic plasma proteome enrichment by Magnetic-COF polymers characterized by (C) enriched peptides amount (yield) with the (D) identified proteins numbers from three independent experiments (n = 3).

(Figure 3A,B and Supporting Table 1), supporting the efficiency of on-bead proteolysis. Binding saturation curves demonstrated that 100 μg of Magnetic-COF sufficed to enrich 125 μL of plasma samples, yielding linear adsorption curves and protein identifications compared with lower and higher Magnetic-COF input (Figure 3C,D and Supporting Table 2). These results establish the optimal conditions for high-efficiency enrichment in automated plasma proteome workflows.

Reproducibility and quantification results were further evaluated by saturation binding analysis. Protein identifications were mostly distributed across intensities between 10^4 and 10^8 among five different binding groups (Figure 4A). Quantitative comparisons showed strong Spearman correlations across 4 replicates in each binding group (Figure 4B), and more than 70% of proteins were reproducibly detected in complete and sparse identifications (Figure 4C). Identified proteins' coefficients of variation (CVs) were generally <25% across intensity ranges, which were divided into 4 categories with protein intensities varying from 10^{10} to 10 (Figure 4D). These findings highlight the robustness of the Magnetic-COF enrichment process, ensuring both the reproducibility and quantitative precision required for proteomics analysis.

Applications for Different Types of Blood Proteomics

To assess versatility across different blood types, plasma, serum, and whole blood samples were processed by an automated enrichment workflow and compared for the proteomics analysis. Plasma samples yielded the largest number of identified proteins, followed by whole blood and serum (Figure 5A and Supporting Tables 3−5). Overlap analysis revealed a substantial shared proteome; alongside fluid-specific proteins, plasma samples showed the most numbers of specific proteins that could be enriched (Figure 5B). The consistent identification of >4000 plasma proteins, >1500 serum proteins, and >4200 whole blood proteins per sample has contributed to exceeding the typical depth achieved without enrichment, which identified 999 plasma proteins (neat results, Figure S3). The different number of proteins identified in plasma compared with those in serum reflects the redistribution of proteins during coagulation in serum collection, particularly those associated with the coagulation cascade, blood microparticles, and extracellular vesicles. In addition, the differences could also reflect the individual differences in blood proteins. GO enrichment analysis comparing enriched plasma and neat plasma demonstrates that neat plasma is dominated by immunoglobulin-, complement-, and coagulation-related categories (Figure S4). At the same time, Magnetic-COF enrichment reduces this dominance and enhances representation of proteins associated with vesicle lumen, secretory granules, cytoplasmic vesicles, and intracellular compartments. The functional diversity is increased without the enrichment of any specific category of proteins. Heatmap clustering further distinguished proteomics signatures among the three matrices with high reproducibility across

https://doi.org/10.1021/acs.analchem.5c08111
Anal. Chem. 2026, 98, 11261−11273

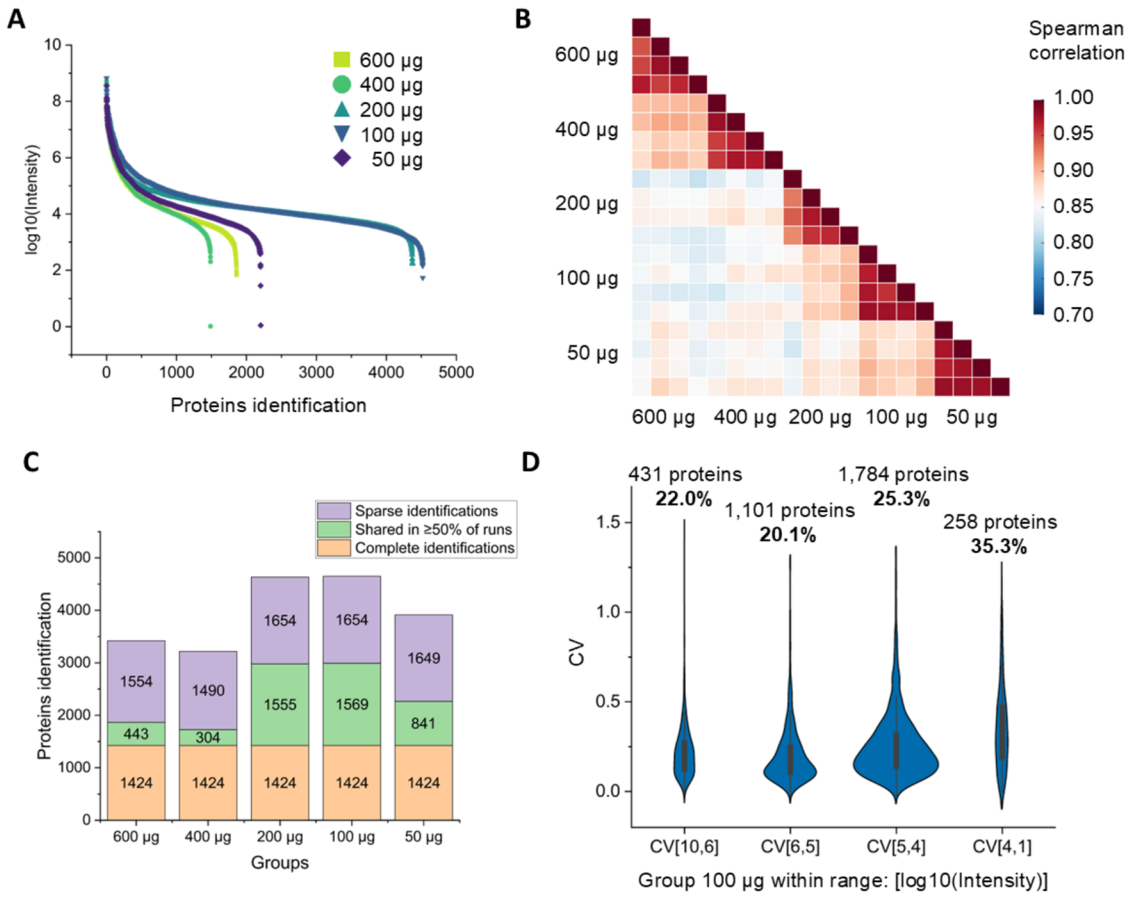

Figure 4. Analytical performance of the plasma protein enrichment by Magnetic-COF. Saturation binding analysis of automatic plasma proteome enrichment by Magnetic-COF polymers characterized by (A) distribution of identified proteins and (B) quantitation results with Spearman correlation heatmap. (C) Proportion of proteins with identification across complete, 50%, and sparse runs among binding groups. (D) Coefficient of variation (CV) for protein measurements across technical replicates from four independently processed PCR wells (n = 4) categorized by the four intensity ranges.

4 replicates (Figure 5C). From the gene ontology cellular component analysis, relatively high-abundant plasma proteins are located at the immunoglobulin complex and blood microparticle. At the same time, relatively high-abundant whole blood proteins were contained by most quantified proteins, located at secretory granule lumen and vesicle lumen. Serum proteins were the least abundant, relatively high-abundance proteins, which were located at the lipoprotein particle. Although Magnetic-COF do not confer specific affinity toward individual low-abundance proteins, they facilitate improved analytical access by mitigating the dominance of high-abundance proteins. This effect arises from the combined contributions of pH-dependent zeta potential, hydrogen bonding, and $\pi-\pi$ interactions from the aromatic COF backbone, together with differential adsorption and desorption behavior during repeated washing steps. Quantitative comparison of representative proteins further supports this mechanism that high-abundance proteins such as albumin and IgG remain dominant and are not amplified after enrichment, whereas low-abundance proteins including MIF and COLEC11 exhibit markedly enhanced signals following Magnetic-COF processing across plasma, serum, and whole blood (Figure S5). To evaluate whether the enrichment introduces systematic physicochemical bias, we analyzed the distributions of molecular weight (Figure S6A), isoelectric point (pI, Figure S6B), hydrophobicity evaluated by the grand average of hydropathy (GRAVY score, Figure S6C), and membrane-bound protein identified with and without enrichment (Figure S6D). These results show that the overall distributions are highly comparable between the enrichment and neat conditions, and a rare bias toward specific molecular weight with median protein mass at 48.3 and 47.2 kDa, pI, or hydrophobicity ranges is observed. The fraction of membrane-associated proteins is not enriched with any preference for subcellular locations (46% and 44%). Compared with neat plasma and previously reported nanomaterial-based enrichment strategies, the Magnetic-COF workflow emphasizes automation compatibility, reproducibility, and scalability while maintaining deep proteome coverage (Table S1). These results demonstrate that this enrichment platform can be adapted to multiple blood sample types, providing flexibility for various clinical and translational applications.

Applications for PDAC Sera Proteomics

Finally, this automatic enrichment platform was applied to the PDAC serum cohort comprising 110 samples (Figure 6 and Supporting Table 6). The overall protein identification across this data set confirmed not only the scalability of the automated Magnetic-COF workflow but also its robustness and reproducibility in a clinical cohort (Figure S7 and Supporting Table 7). Importantly, comparable numbers of around 1600 of identified proteins were obtained across samples spanning a wide dynamic range of protein abundance

https://doi.org/10.1021/acs.analchem.5c08111
Anal. Chem. 2026, 98, 11261−11273

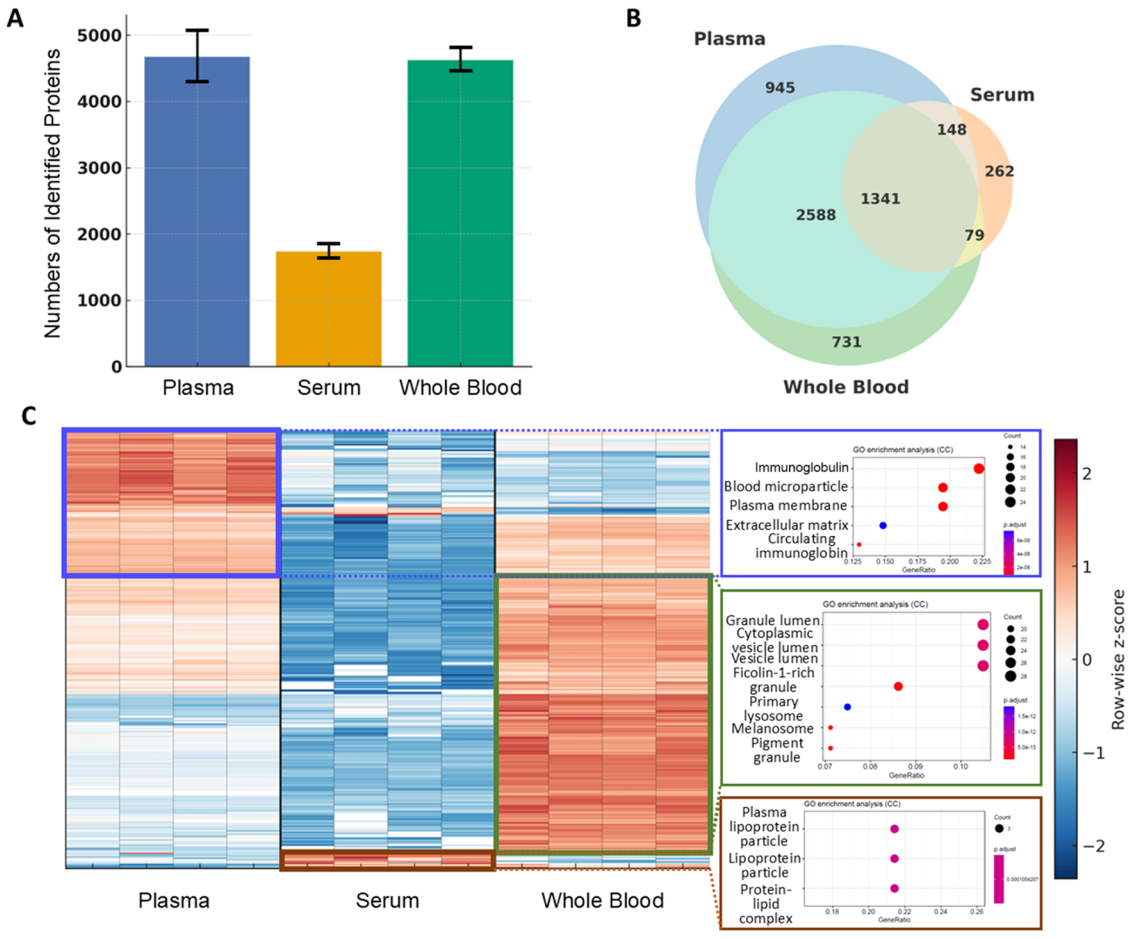

Figure 5. Enrichment of Different Types of Blood Samples using Magnetic-COF for Blood Proteomics. Comparative performance of the automated Magnetic-COF methods applied in plasma, serum, and whole blood proteomics. (A) Bar plot showing the number of proteins identified from each biofluid type across human plasma, serum, and whole blood. (B) Venn diagram illustrates the overlap and unique protein identifications among the three sample types. (C) Heatmap of representative protein quantification results with clustered across 4 replicates. Most abundant groups were analyzed by gene ontology (GO) enrichment analysis, cellular component (CC).

by combined database searches, representing an approximate 72% improvement in single-run serum proteome depth and indicating that the automated enrichment and digestion steps remained stable and reproducible under cohort-scale operation (Supporting Table 8). Protein-level CV of pooled QC samples showed that between-batch variability (17.9%) was comparable to within-batch variability (16.1% for plate #1 and 22.2% for plate #2), indicating minimal batch effects across the quantification results in the PDAC sera proteome. Comparative analysis between PDAC and matched control samples revealed significantly altered proteins (Figure 6A), many of which have functional links to cancer biology. Fold-change analyses across 55 PDAC and non-PDAC serum samples highlighted consistent differences for selected proteins APOE, CEACAM5, OTC, and ECHDC3 (Figure 6B−E). The consistent upregulation of APOE and CEACAM5 across both PDAC tumor serum and tissue proteomic data sets suggests that these proteins are robustly associated with the molecular landscape of PDAC via lipid metabolism, extracellular remodeling, and tumor−immune interactions.[15] APOE, a lipid-transport and immune-modulatory apolipoprotein primarily synthesized in the liver and macrophages, has recently gained attention for its role in the tumor microenvironment.[32] Elevated APOE expression in PDAC tissues and circulation likely reflects metabolic reprogramming and lipid-signaling alterations that accompany malignant transformation.[33] APOE can promote cholesterol efflux, oxidative stress modulation, and cell-surface receptor signaling LRP1, processing that support tumor growth and immune evasion.[34] Recent studies have shown that APOE is upregulated in PDAC and correlates with poor prognosis, enhanced cell migration, and immune suppression through macrophage polarization and extracellular matrix remodeling.[35] CEACAM5, also known as carcinoembryonic antigen (CEA), is a well-known cell-adhesion glycoprotein overexpressed in several epithelial cancers, including pancreatic, colorectal, and gastric carcinomas.[36] CEACAM5 plays crucial roles in cell−cell adhesion, metastasis, and immune modulation, often contributing to tumor cell detachment and dissemination.[37] Its overexpression in PDAC tissue aligns with prior histopathological and transcriptomic observations, where CEA family proteins were enriched in ductal and invasive regions of pancreatic tumors.[15] The concurrent elevation of CEACAM5 in serum reflects tumor-derived shedding of glycoproteins into the bloodstream, a phenomenon exploited clinically for CEA-based diagnostic assays.[38] The simultaneous elevation of APOE and CEACAM5 in both tissue and serum underscores a broader pathophysiological axis in PDAC that couples lipid metabolism, extracellular remodeling, and tumor−immune interactions. It supports the notion that integrating tissue and serum

https://doi.org/10.1021/acs.analchem.5c08111
Anal. Chem. 2026, 98, 11261−11273

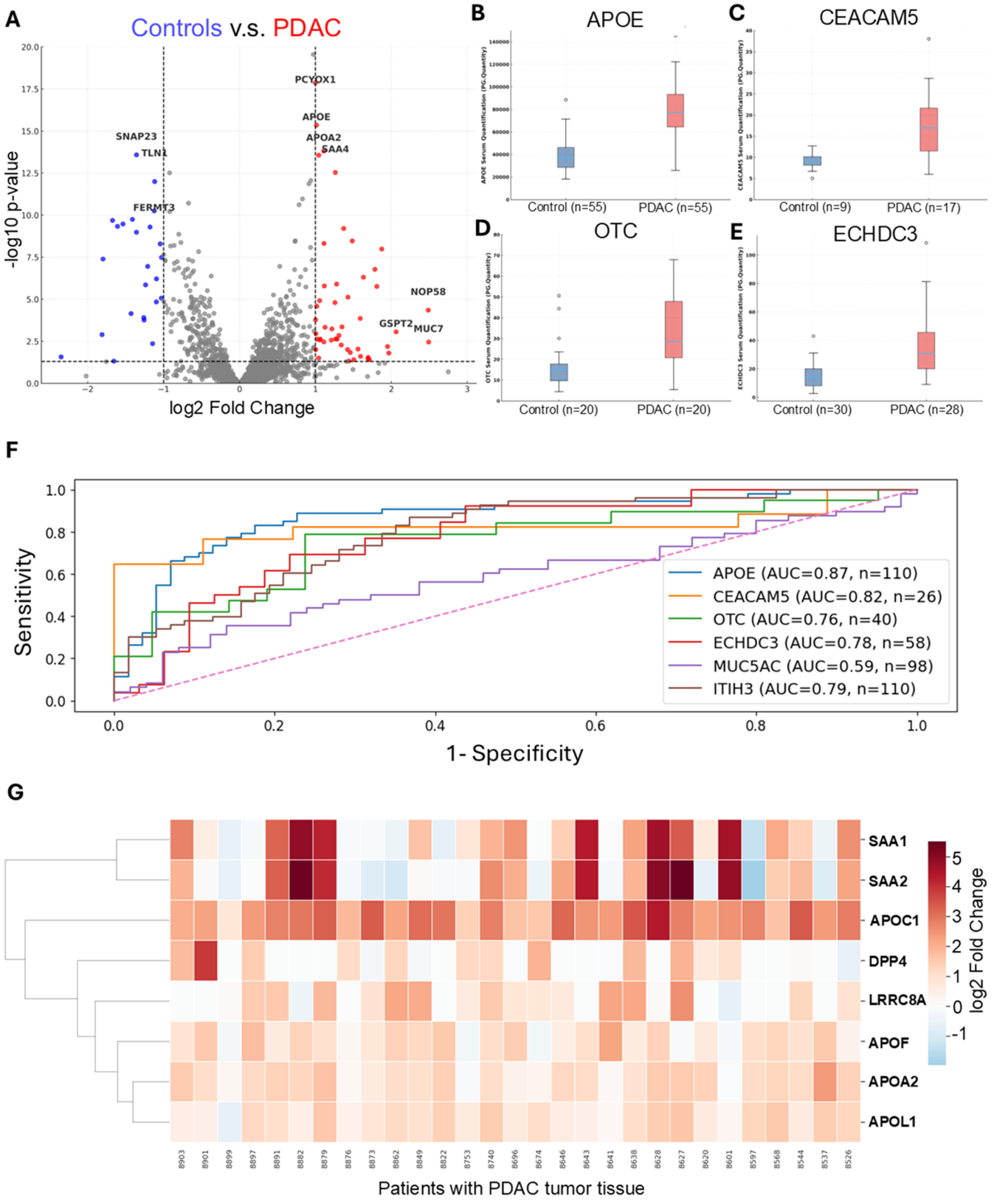

Figure 6. Application of the automated Magnetic-COF workflow in pancreatic ductal adenocarcinoma (PDAC) serum proteomics. (A) Volcano plot showing significantly up- and downregulated proteins between 55 PDAC serum and 55 control serum samples (red: upregulated; blue: downregulated; gray: nonsignificant). (B–E) Fold-change boxplots of proteins APOE, CEACAM5, OTC, and ECHDC3 across 55 PDAC and 55 control serum samples. (F) Receiver operating characteristic (ROC) curves showing the diagnostic performance of selected differential proteins (APOE, CEACAM5, OTC, ECHDC3, and MUC5AC) for distinguishing PDAC from control serum samples based on protein-level quantitative intensities in PDAC serum proteomics enriched by Magnetic-COF. (G) Heatmap of $\log_2$ fold changes for proteins APOA2, APOC1, APOF, APOL1, DPP4, LRRC8A, SAA1, and SAA2 across 29 of PDAC patient samples that matched tumor-tissue samples and compared with the disease-

https://doi.org/10.1021/acs.analchem.5c08111
Anal. Chem. 2026, 98, 11261−11273

Figure 6. continued

free control group. Differential proteins were screened by using two-sided *t* tests with Benjamini−Hochberg correction (FDR < 0.05) and an absolute $\log_2$ fold-change ≥ 1.

proteomics can identify translatable protein candidates. While OTC and ECHDC3 are upregulated in PDAC serum but downregulated in tumor tissue, this suggests a complex regulatory pattern reflecting metabolic disruption, tissue leakage, and altered mitochondrial activity in pancreatic cancer. OTC, a mitochondrial enzyme critical for the urea cycle, catalyzes the conversion of ornithine and carbamoyl phosphate to citrulline, thereby regulating nitrogen metabolism and ammonia detoxification.[39] Its downregulation in PDAC tissues reflects suppressed hepatic-like metabolic functions and the mitochondrial dysfunction commonly observed in pancreatic tumors.[40] Tumor cells often downregulate OTC and other urea-cycle enzymes to divert nitrogen toward biosynthetic pathways that support proliferation.[41] However, the increased levels of OTC detected in serum arise from cellular release or leakage due to tissue necrosis, mitochondrial stress, or damage-associated protein shedding.[42] Elevated circulating OTC has also been linked to hepatic injury and altered nitrogen metabolism, which was regarded as a systemic response to PDAC-related cachexia and metabolic stress.[43] This pattern indicates that serum OTC may serve as a secondary marker of PDAC-associated metabolic disturbance rather than direct tumor secretion. ECHDC3, a mitochondrial enzyme involved in fatty acid β-oxidation and ethylmalonate metabolism,[44] exhibits a similar phenomenon that decreased in PDAC tissue but elevated in serum. Tumor-tissue downregulation of ECHDC3 aligns with a shift toward glycolytic metabolism and suppression of mitochondrial oxidative pathways.[45] Reduced ECHDC3 supported lipid accumulation and redox adaptation within the tumor microenvironment.[46] Conversely, the elevated serum ECHDC3 reflects a systemic metabolic response and release from normal pancreatic tissues under PDAC-induced metabolic stress. This systemic upregulation could represent compensatory activation of peripheral fatty acid oxidation to maintain the metabolic balance during tumor progression. To evaluate the diagnostic performance of these identified differential proteins, receiver operating characteristic (ROC) analysis was generated for APOE, CEACAM5, OTC, ECHDC3, and MUC5AC based on protein-level quantitative intensities across PDAC and control samples (Figure 6F). APOE and CEACAM5 demonstrated strong discriminatory performance (AUC = 0.87 and 0.82, respectively), while ITIH3, OTC, and ECHDC3 showed moderate classification accuracy (AUC = 0.79, 0.76, and 0.78). In contrast, MUC5AC exhibited limited diagnostic performance (AUC = 0.59), consistent with the glycan-dependent nature of CA19−9−associated mucins.

From the 29 tumor-tissue-matched serum samples,[16] APOA2, APOC1, APOF, APOL1, DPP4, LRRC8A, SAA1, and SAA2 were quantified to be upregulated in the PDAC group (Figure 6G). Apolipoprotein A-II (APOA2) is the second-most abundant apolipoprotein of high-density lipoproteins (HDL) and plays a key role in lipid metabolism, cholesterol transport, and regulation of lipoprotein structure.[47] In PDAC, elevated expression of APOA2 has been repeatedly observed in serum due to altered lipid metabolism in cancer.[48] Dysregulation of apolipoprotein APOA2 reflects and drives the metabolic reprogramming that sustains tumor growth.[49] High serum APOA2 levels have been proposed as part of multimarker panels for PDAC detection.[50] Truncated isoforms of APOA2 (APOA2-ATQ/AT, APOA2-AT/AT) have been studied as biomarkers to discriminate PDAC from healthy individuals or patients with chronic pancreatitis.[51] Apolipoprotein C−I (APOC1) is a small apolipoprotein primarily associated with very-low-density (VLDL) and high-density lipoprotein (HDL), where it regulates triglyceride and cholesterol metabolism.[52] Elevated APOC1 expression in serum proteomics exacerbates the pro-inflammatory milieu characteristic of PDAC, contributing to immune evasion and tumor progression.[53] Apolipoprotein F (APOF), also known as lipid transfer inhibitor protein, is a minor plasma apolipoprotein predominantly associated with low-density lipoproteins (LDL) and HDL.[54] Its main function is to modulate lipid transfer protein (CETP) activity, thereby influencing cholesterol ester transport and lipid exchange between lipoprotein particles.[55] In PDAC, increased serum levels of APOF reflect a host response to metabolic stress, where hepatic production of apolipoproteins is modified as part of the acute-phase and metabolic reprogramming responses.[56] As an HDL-associated protein, APOL1 regulates cholesterol efflux and phospholipid metabolism.[57] High circulating APOL1 reflects enhanced lipid remodeling, consistent with the increased energy and membrane synthesis demands of PDAC cells.[58] APOL1 has been implicated in autophagy and programmed cell death.[59] Aberrant overexpression in PDAC contributes to dysregulated cell survival pathways, favoring tumor persistence under stress conditions.[60] Dipeptidyl peptidase 4 (DPP4, also known as CD26) is a membrane-bound serine protease that cleaves N-terminal dipeptides from a wide range of bioactive peptides, including incretins, chemokines, and growth factors.[61] While DPP4 is normally expressed on epithelial cells and immune cells, elevated serum levels and increased enzymatic activity have been observed in PDAC.[62] DPP4 regulates chemokine CXCL12/SDF-1α activity, thereby controlling T cell trafficking and immune surveillance.[63] High expression of DPP4 impairs effective antitumor immune responses and facilitates immune evasion.[64] Leucine-rich repeat-containing protein 8A (LRRC8A) is an essential subunit of volume-regulated anion channels (VRACs), which regulate cell volume, chloride conductance, and transport of organic osmolytes.[65] Aberrant LRRC8A expression shifts this balance to favor survival and proliferation, supporting PDAC growth despite hostile microenvironmental conditions.[66] Serum amyloid A proteins (SAA1 and SAA2) are acute-phase reactants predominantly synthesized in the liver and secreted into circulation in response to pro-inflammatory cytokines such as IL-1, IL-6, and TNF-α.[67] Under normal conditions, their plasma concentrations are very low, but during systemic inflammation, they can increase by more than a thousand-fold.[68] In pancreatic ductal adenocarcinoma (PDAC), high serum levels of SAA1 and SAA2 are strongly induced by inflammatory cytokines, and their upregulation reflects systemic and local inflammation associated with the tumor.[69] Elevated SAAs can act as a chemoattractant for immune cells, reinforcing the pro-tumor inflammatory milieu, promoting matrix metalloproteinase (MMP) expression, and facilitating extracellular matrix

https://doi.org/10.1021/acs.analchem.5c08111
Anal. Chem. 2026, 98, 11261−11273

degradation.[70] This activity may enhance the invasive and metastatic potential of PDAC cells, which is consistent with the highly aggressive clinical course of the disease.

These data demonstrate the clinical relevance of the Magnetic-COF workflow, enabling robust, large-scale identification of disease-associated proteins in PDAC serum.

CONCLUSIONS

This work presents an automated plasma proteome enrichment and analysis platform integrating magnetic covalent organic frameworks (Magnetic-COF) with robotic liquid handling. The system combines high molecular selectivity, tunable porosity, and magnetic separability to achieve efficient capture and on-bead digestion of plasma proteins with high reproducibility. Under optimized conditions, the workflow identified more than 4000 proteins per sample with consistent performance across plasma, serum, and whole blood, processing up to 30 samples per day. Structural and kinetic analyses confirmed that Magnetic-COF maintained stability, reversible pore responsiveness, and favorable adsorption dynamics, supporting their suitability for large-scale proteomics. Automated sample handling using the Opentrons OT-2 platform minimized manual variation and improved quantitation precision, with coefficients of variation typically below 25%. Application of this workflow to 110 serum samples from patients with pancreatic ductal adenocarcinoma (PDAC) demonstrated its capacity for high-throughput clinical proteomics. Differential expression profiling revealed reproducible alterations in apolipoproteins, cell-adhesion molecules, and metabolic enzymes, illustrating the analytical robustness and biological relevance of the platform.

In summary, the magnetic-COF–based automated system provides a reproducible, high-throughput, and adaptable solution for plasma and serum proteomics. Its integration of magnetic nanomaterials with robotic automation overcomes the key limitations of manual enrichment workflows and establishes a scalable foundation for clinical biomarker discovery and translational proteomics studies.

ASSOCIATED CONTENT

Data Availability Statement

The database and related tools are openly accessible by PRIDE repository PXD071659.

Supporting Information

The Supporting Information is available free of charge at https://pubs.acs.org/doi/10.1021/acs.analchem.5c08111.

Table, figures, and automatic blood proteome enrichment (PDF)

Quantification of proteins identified by automatic blood proteome enrichment by Magnetic-COF polymers with trypsin digestion time gradient, different input beads amount, quantification of proteins identified in plasma, whole blood and serum samples, PDAC serum samples information, identification and quantification of proteins (XLSX)

AUTHOR INFORMATION

Corresponding Author

Hui Zhang − *Department of Pathology, Johns Hopkins University School of Medicine, Baltimore, Maryland 21205, United States;* orcid.org/0000-0001-8726-7098; Email: huizhang@jhu.edu

Authors

Yuanyu Huang − *Department of Pathology, Johns Hopkins University School of Medicine, Baltimore, Maryland 21205, United States;* orcid.org/0009-0002-5930-8424

T. Mamie Lih − *Department of Pathology, Johns Hopkins University School of Medicine, Baltimore, Maryland 21205, United States;* orcid.org/0000-0003-0317-2660

Zhenyu Sun − *Department of Pathology, Johns Hopkins University School of Medicine, Baltimore, Maryland 21205, United States;* orcid.org/0009-0002-5004-5904

Liyuan Jiao − *Department of Pathology, Johns Hopkins University School of Medicine, Baltimore, Maryland 21205, United States*

Lijun Chen − *Department of Pathology, Johns Hopkins University School of Medicine, Baltimore, Maryland 21205, United States*

Complete contact information is available at: https://pubs.acs.org/10.1021/acs.analchem.5c08111

Author Contributions

The manuscript was written through contributions of all authors. All authors have given approval to the final version of the manuscript.

Notes

The authors declare no competing financial interest.

ACKNOWLEDGMENTS

This work was supported by National Institutes of Health, National Cancer Institute, the Clinical Proteomic Tumor Analysis Consortium (CPTAC, U24CA271079), the Early Detection Research Network (EDRN, U2CCA271895), Pancreatic Cancer Detection Consortium (PCDC, U01CA274514).

ABBREVIATIONS

APOA2, apolipoprotein A-II; APOC1, apolipoprotein C−I; APOF, apolipoprotein F; APOL1, apolipoprotein L1; BD, Becton, Dickinson and Company; CEA, carcinoembryonic antigen; CEACAM5, carcinoembryonic antigen−related cell adhesion molecule 5; COFs, covalent organic frameworks; CV, coefficient of variation; DIA, data-independent acquisition; DIA-MS, data-independent acquisition mass spectrometry; DMTA, 2,5-dimethoxybenzene-1,4-dicarbaldehyde; DPP4, dipeptidyl peptidase 4; DTT, dithiothreitol; ECHDC3, enoyl-CoA hydratase domain−containing protein 3; EV-1000, Evosep One EV-1000 system; FA, formic acid; FDR, false discovery rate; Fe_3O_4, iron(II,III) oxide (magnetite); GI/HPB, gastrointestinal/hepatopancreatobiliary; GO, gene ontology; HDL, high-density lipoprotein; HREBA, Health Research Ethics Board of Alberta; IAA, iodoacetamide; LC-MS/MS, liquid chromatography−tandem mass spectrometry; LDL, low-density lipoprotein; LRRC8A, leucine-rich repeat−containing protein 8A; Lys-C, endoproteinase Lys-C; Magnetic-COF, magnetic covalent organic frameworks; MMP, matrix metalloproteinase; MS, mass spectrometry; OT-2, Opentrons OT-2 liquid-handling robot; OTC, ornithine transcarbamylase; PCR, polymerase chain reaction; PDAC, pancreatic ductal adenocarcinoma; PRIDE, Proteomics Identifications Database; SAA1, serum amyloid A1; SAA2, serum amyloid A2; SPD,

https://doi.org/10.1021/acs.analchem.5c08111
Anal. Chem. 2026, 98, 11261−11273

samples per day; TAPB, 1,3,5-tri-(4-aminophenyl)benzene; TEM, transmission electron microscopy; Tris-HCl, tris-(hydroxymethyl)aminomethane hydrochloride; VLDL, very-low-density lipoprotein; VRAC, volume-regulated anion channel.

REFERENCES

(1) Sun, B. B.; Maranville, J. C.; Peters, J. E.; Stacey, D.; Staley, J. R.; Blackshaw, J.; Burgess, S.; Jiang, T.; Paige, E.; Surendran, P.; Oliver-Williams, C.; Kamat, M. A.; Prins, B. P.; Wilcox, S. K.; Zimmerman, E. S.; Chi, A.; Bansal, N.; Spain, S. L.; Wood, A. M.; Morrell, N. W.; Bradley, J. R.; Janjic, N.; Roberts, D. J.; Ouwehand, W. H.; Todd, J. A.; Soranzo, N.; Suhre, K.; Paul, D. S.; Fox, C. S.; Plenge, R. M.; Danesh, J.; Runz, H.; Butterworth, A. S. Genomic atlas of the human plasma proteome. *Nature* **2018**, *558*, 73−79.

(2) Kalinich, M.; Haber, D. A. Cancer detection: Seeking signals in blood. *Science* **2018**, *359*, 866−867.

(3) Malmström, E.; Malmström, L.; Hauri, S.; Mohanty, T.; Scott, A.; Karlsson, C.; Gueto-Tettay, C.; Åhrman, E.; Nozohoor, S.; Tingstedt, B.; Regner, S.; Elfving, P.; Bjermer, L.; Forsvall, A.; Doyle, A.; Magnusson, M.; Hedenfalk, I.; Kannisto, P.; Brandt, C.; Nilsson, E.; Dahlin, L. B.; Malm, J.; Linder, A.; Niméus, E.; Malmström, J. Human proteome distribution atlas for tissue-specific plasma proteome dynamics. *Cell* **2025**, *188*, 2810−2822.

(4) Zhang, H.; Chan, D. W. Cancer Biomarker Discovery in Plasma Using a Tissue-targeted Proteomic Approach. *Cancer Epidemiol., Biomarkers Prev.* **2007**, *16*, 1915−1917.

(5) Papier, K.; Atkins, J. R.; Tong, T. Y. N.; Gaitskell, K.; Desai, T.; Ogamba, C. F.; Parsaeian, M.; Reeves, G. K.; Mills, I. G.; Key, T. J.; Smith-Byrne, K.; Travis, R. C. Identifying proteomic risk factors for cancer using prospective and exome analyses of 1463 circulating proteins and risk of 19 cancers in the UK Biobank. *Nat. Commun.* **2024**, *15*, No. 4010, DOI: 10.1038/s41467-024-48017-6.

(6) Shaw, J. R.; Caprio, N.; Truong, N.; Weldemariam, M.; Tran, A.; Pilli, N.; Pandey, S.; Jones, J. W.; Kane, M. A.; Pearson, R. M. Inflammatory disease progression shapes nanoparticle biomolecular corona-mediated immune activation profiles. *Nat. Commun.* **2025**, *16*, No. 924, DOI: 10.1038/s41467-025-56210-4.

(7) Malmström, E.; Kilsgård, O.; Hauri, S.; Smeds, E.; Herwald, H.; Malmström, L.; Malmström, J. Large-scale inference of protein tissue origin in gram-positive sepsis plasma using quantitative targeted proteomics. *Nat. Commun.* **2016**, *7*, No. 10261, DOI: 10.1038/ncomms10261.

(8) Eissa, T.; Leonardo, C.; Kepesidis, K. V.; Fleischmann, F.; Linkohr, B.; Meyer, D.; Zoka, V.; Huber, M.; Voronina, L.; Richter, L.; Peters, A.; Žigman, M. Plasma infrared fingerprinting with machine learning enables single-measurement multi-phenotype health screening. *Cell Rep. Med.* **2024**, *5* (7), No. 101625, DOI: 10.1016/j.xcrm.2024.101625.

(9) Huang, Z.; Yan, G.; Gao, M.; Zhang, X. Array-Based Online Two Dimensional Liquid Chromatography System Applied to Effective Depletion of High-Abundance Proteins in Human Plasma. *Anal. Chem.* **2016**, *88*, 2440−2445.

(10) Tamburro, D.; Fredolini, C.; Espina, V.; Douglas, T. A.; Ranganathan, A.; Ilag, L.; Zhou, W.; Russo, P.; Espina, B. H.; Muto, G.; Petricoin, E. F.; Liotta, L. A.; Luchini, A. Multifunctional Core−Shell Nanoparticles: Discovery of Previously Invisible Biomarkers. *J. Am. Chem. Soc.* **2011**, *133*, No. 19178.

(11) Bai, L.; Lyu, J.; Feng, J.; Qiao, X.; Qu, Y.; Yang, G.; Zhu, Y.; Liao, L.; Gao, H.; Zang, A.; Xu, Z.; Ji, T.; Ran, P.; Ding, W.; Zhang, H.; Zhu, L.; Wang, Y.; Wang, L.; Wang, X.; Li, Y.; Li, J.; Yin, X.; Zhao, G.; Liu, D.; Gao, X.; Tian, S.; Tan, S.; Pu, Y.; Li, L.; Song, Z.; Song, J.; Guo, W.; Liao, Y.; Ye, D.; Yang, W.; Jia, Y.; Ding, C. Cancer biomarkers discovered using pan-cancer plasma proteomic profiling. *Nat. Biomed. Eng.* **2026**, *10* (1), 16−38, DOI: 10.1038/s41551-025-01448-y.

(12) Leiphrakpam, P. D.; Chowdhury, S.; Zhang, M.; Bajaj, V.; Dhir, M.; Are, C. Trends in the Global Incidence of Pancreatic Cancer and a Brief Review of its Histologic and Molecular Subtypes. *J. Gastrointest. Cancer* **2025**, *56*, 71−72.

(13) Siegel, R. L.; Kratzer, T. B.; Giaquinto, A. N.; Sung, H.; Jemal, A. Cancer statistics, 2025. *Ca-Cancer J. Clin.* **2025**, *75*, No. 10.

(14) Brand, R. E.; Nolen, B. M.; Zeh, H. J.; Allen, P. J.; Eloubeidi, M. A.; Goldberg, M.; Elton, E.; Arnoletti, J. P.; Christein, J. D.; Vickers, S. M.; Langmead, C. J.; Landsittel, D. P.; Whitcomb, D. C.; Grizzle, W. E.; Lokshin, A. E. Serum Biomarker Panels for the Detection of Pancreatic Cancer. *Clin. Cancer Res.* **2011**, *17*, 805−816.

(15) Cao, L.; Huang, C.; Cui Zhou, D.; Hu, Y.; Lih, T. M.; Savage, S. R.; Krug, K.; Clark, D. J.; Schnaubelt, M.; Chen, L.; Da Veiga Leprevost, F.; Eguez, R. V.; Yang, W.; Pan, J.; Wen, B.; Dou, Y.; Jiang, W.; Liao, Y.; Shi, Z.; Terekhanova, N. V.; Cao, S.; Lu, R. J.; Li, Y.; Liu, R.; Zhu, H.; Ronning, P.; Wu, Y.; Wyczalkowski, M. A.; Easwaran, H.; Danilova, L.; Mer, A. S.; Yoo, S.; Wang, J. M.; Liu, W.; Haibe-Kains, B.; Thiagarajan, M.; Jewell, S. D.; Hostetter, G.; Newton, C. J.; Li, Q. K.; Roehrl, M. H.; Fenyö, D.; Wang, P.; Nesvizhskii, A. I.; Mani, D. R.; Omenn, G. S.; Boja, E. S.; Mesri, M.; Robles, A. I.; Rodriguez, H.; Bathe, O. F.; Chan, D. W.; Hruban, R. H.; Ding, L.; Zhang, B.; Zhang, H.; Amin, M.; An, E.; Ayad, C.; Bauer, T.; Birger, C.; Birrer, M. J.; Boca, S. M.; Bocik, W.; Borucki, M.; Cai, S.; Carr, S. A.; Cerda, S.; Chen, H.; Chen, S.; Chesla, D.; Chinnaiyan, A. M.; Colaprico, A.; Cottingham, S.; Derejska, M.; Dhanasekaran, S. M.; Domagalski, M. J.; Druker, B. J.; Duffy, E.; Dyer, M. A.; Edwards, N. J.; Ellis, M. J.; Eschbacher, J.; Francis, A.; Francis, J.; Gabriel, S.; Gabrovski, N.; Gardner, J.; Getz, G.; Gillette, M. A.; Goldthwaite, C. A.; Grady, P.; Guo, S.; Hariharan, P.; Hiltke, T.; Hindenach, B.; Hoadley, K. A.; Huang, J.; Jones, C. D.; Ketchum, K. A.; Kinsinger, C. R.; Koziak, J. M.; Kusnierz, K.; Liu, T.; Long, J.; Mallery, D.; Mareedu, S.; Matteotti, R.; Maunganidze, N.; Mcgarvey, P. B.; Minoo, P.; Paklina, O. V.; Paulovich, A. G.; Payne, S. H.; Potapova, O.; Pruetz, B.; Qi, L.; Roche, N.; Rodland, K. D.; Rohrer, D. C.; Schadt, E. E.; Shabunin, A. V.; Shelton, T.; Shutack, Y.; Singh, S.; Smith, M.; Smith, R. D.; Sokoll, L. J.; Suh, J.; Thangudu, R. R.; Tsang, S. X.; Um, K. S.; Valley, D. R.; Vatanian, N.; Wang, W.; Wilson, G. D.; Wiznerowicz, M.; Zhang, Z.; Zhao, G. Proteogenomic characterization of pancreatic ductal adenocarcinoma. *Cell* **2021**, *184*, 5031−5032.

(16) Lih, T. M.; Cao, L.; Minoo, P.; Omenn, G. S.; Hruban, R. H.; Chan, D. W.; Bathe, O. F.; Zhang, H. Detection of Pancreatic Ductal Adenocarcinoma-Associated Proteins in Serum. *Molecular & amp Cellular Proteomics* **2024**, *23* (1), No. 100687, DOI: 10.1016/j.mcpro.2023.100687.

(17) Huang, P.; Gao, W.; Fu, C.; Wang, M.; Li, Y.; Chu, B.; He, A.; Li, Y.; Deng, X.; Zhang, Y.; Kong, Q.; Yuan, J.; Wang, H.; Shi, Y.; Gao, D.; Qin, R.; Hunter, T.; Tian, R. Clinical functional proteomics of intercellular signalling in pancreatic cancer. *Nature* **2025**, *637*, 726−735.

(18) Di Marco, F.; Cufaro, M. C.; Damiani, V.; Dufrusine, B.; Pizzinato, E.; Di Ferdinando, F.; Sala, G.; Lattanzio, R.; Dainese, E.; Federici, L.; Ponsaerts, P.; De Laurenzi, V.; Cicalini, I.; Pieragostino, D. Proteomic meta-analysis unveils new frontiers for biomarkers research in pancreatic carcinoma. *Oncogenesis* **2025**, *14* (1), No. 3, DOI: 10.1038/s41389-025-00547-4.

(19) Smith-Byrne, K.; Hedman, Å.; Dimitriou, M.; Desai, T.; Sokolov, A. V.; Schioth, H. B.; Koprulu, M.; Pietzner, M.; Langenberg, C.; Atkins, J.; Penha, R. C.; Mckay, J.; Brennan, P.; Zhou, S.; Richards, B. J.; Yarmolinsky, J.; Martin, R. M.; Borlido, J.; Mu, X. J.; Butterworth, A.; Shen, X.; Wilson, J.; Assimes, T. L.; Hung, R. J.; Amos, C.; Purdue, M.; Rothman, N.; Chanock, S.; Travis, R. C.; Johansson, M.; Mälarstig, A. Identifying therapeutic targets for cancer among 2074 circulating proteins and risk of nine cancers. *Nat. Commun.* **2024**, *15*, No. 3621, DOI: 10.1038/s41467-024-46834-3.

(20) Soragni, A.; Knudsen, E. S.; O'connor, T. N.; Tognon, C. E.; Tyner, J. W.; Gini, B.; Kim, D.; Bivona, T. G.; Zang, X.; Witkiewicz, A. K.; Goodrich, D. W.; Jiang, D.; Gammon, S. T.; Willey, C. D.; Boutros, P. C.; Sandulache, V. C.; Osman, A. A.; Myers, J. N.; Mehla, K.; Singh, P. K.; Chan, K. S.; Gao, H.; Marathe, H. Acquired resistance in cancer: towards targeted therapeutic strategies. *Nat. Rev. Cancer* **2025**, *25* (8), 613−633, DOI: 10.1038/s41568-025-00824-9.

https://doi.org/10.1021/acs.analchem.5c08111
Anal. Chem. 2026, 98, 11261−11273

(21) Na, T.-Y.; Schecterson, L.; Mendonsa, A. M.; Gumbiner, B. M. The functional activity of E-cadherin controls tumor cell metastasis at multiple steps. *Proc. Natl. Acad. Sci. U.S.A.* **2020**, *117*, 5931−5937.
(22) Schuster, E.; Taftaf, R.; Reduzzi, C.; Albert, M. K.; Romero-Calvo, I.; Liu, H. Better together: circulating tumor cell clustering in metastatic cancer. *Trends Cancer* **2021**, *7*, 1020−1032.
(23) Chang, T.-G.; Park, S.; Schäffer, A. A.; Jiang, P.; Ruppin, E. Hallmarks of artificial intelligence contributions to precision oncology. *Nat. Cancer* **2025**, *6* (3), 417−431.
(24) Tavoosidana, G.; Ronquist, G.; Darmanis, S.; Yan, J.; Carlsson, L.; Wu, D.; Conze, T.; Ek, P.; Semjonow, A.; Eltze, E.; Larsson, A.; Landegren, U. D.; Kamali-Moghaddam, M. Multiple recognition assay reveals prostasomes as promising plasma biomarkers for prostate cancer. *Proc. Natl. Acad. Sci. U.S.A.* **2011**, *108*, 8809−8814.
(25) Wang, J.; Xie, W.; Sun, L.; Li, J.; Wu, S.; Li, R.; Zhao, Y. Establishment and clinical application evaluations of a deep mining strategy of plasma proteomics based on nanomaterial protein coronas. *Anal. Chim. Acta* **2023**, *1275*, No. 341569, DOI: 10.1016/j.aca.2023.341569.
(26) Beimers, W. F.; Overmyer, K. A.; Sinitcyn, P.; Lancaster, N. M.; Quarmby, S. T.; Coon, J. J. Technical Evaluation of Plasma Proteomics Technologies. *J. Proteome Res.* **2025**, *24*, 3074−3087.
(27) Zhu, Y.; Wang, X.; Wu, M. Intriguing Room Temperature Phosphorescence in Crystalline Porous Organic Frameworks. *Adv. Funct Mater.* **2023**, *33*, No. 2308096, DOI: 10.1002/adfm.202308096.
(28) Li, Z.; Paitandi, R. P.; Tsutsui, Y.; Matsuda, W.; Nobuoka, M.; Chen, B.; Ghosh, S.; Tanaka, T.; Suda, M.; Zhu, T.; Kageyama, H.; Miyake, Y.; Shinokubo, H.; Takagi, M.; Shimazaki, T.; Tachikawa, M.; Suzuki, K.; Kaji, H.; Ando, Y.; Ezaki, T.; Seki, S. Rolling two-dimensional covalent organic framework (COF) sheets into one-dimensional electronic and proton-conductive nanotubes. *Proc. Natl. Acad. Sci. U.S.A.* **2025**, *122* (16), No. e2424314122, DOI: 10.1073/pnas.2424314122.
(29) Zhang, J.; Li, Y.; Li, J.; Zhu, L.; Jin, S. Biomimetic synthesis of vesicular covalent organic frameworks by gemini surfactants for in-situ enzyme cascade immobilization. *Nat. Commun.* **2025**, *16*, No. 6046, DOI: 10.1038/s41467-025-60719-z.
(30) Emmerling, S. T.; Schuldt, R.; Bette, S.; Yao, L.; Dinnebier, R. E.; Kästner, J.; Lotsch, B. V. Interlayer Interactions as Design Tool for Large-Pore COFs. *J. Am. Chem. Soc.* **2021**, *143*, No. 15711.
(31) Qing, Q.; Luo, J.; Liu, S.; Wang, J.; Wang, Z.; Xiong, X.; Chen, J.; Lu, Y. General synthesis of covalent organic frameworks under ambient condition within minutes via microplasma electrochemistry approach. *Nat. Commun.* **2025**, *16* (1), No. 2571, DOI: 10.1038/s41467-025-57892-6.
(32) Tavazoie, M. F.; Pollack, I.; Tanqueco, R.; Ostendorf, B. N.; Reis, B. S.; Gonsalves, F. C.; Kurth, I.; Andreu-Agullo, C.; Derbyshire, M. L.; Posada, J.; Takeda, S.; Tafreshian, K. N.; Rowinsky, E.; Szarek, M.; Waltzman, R. J.; Mcmillan, E. A.; Zhao, C.; Mita, M.; Mita, A.; Chmielowski, B.; Postow, M. A.; Ribas, A.; Mucida, D.; Tavazoie, S. F. LXR/ApoE Activation Restricts Innate Immune Suppression in Cancer. *Cell* **2018**, *172*, 825−840.
(33) Zhang, J.; Song, J.; Tang, S.; Zhao, Y.; Wang, L.; Luo, Y.; Tang, J.; Ji, Y.; Wang, X.; Li, T.; Zhang, H.; Shao, W.; Sheng, J.; Liang, T.; Bai, X. Multi-omics analysis reveals the chemoresistance mechanism of proliferating tissue-resident macrophages in PDAC via metabolic adaptation. *Cell Rep.* **2023**, *42* (6), No. 112620, DOI: 10.1016/j.celrep.2023.112620.
(34) Rauch, J. N.; Luna, G.; Guzman, E.; Audouard, M.; Challis, C.; Sibih, Y. E.; Leshuk, C.; Hernandez, I.; Wegmann, S.; Hyman, B. T.; Gradinaru, V.; Kampmann, M.; Kosik, K. S. LRP1 is a master regulator of tau uptake and spread. *Nature* **2020**, *580*, 381−385.
(35) Gulhati, P.; Schalck, A.; Jiang, S.; Shang, X.; Wu, C.; Hou, P.; Ruiz, S. H.; Soto, L. S.; Parra, E.; Ying, H.; Han, J.; Dey, P.; Li, J.; Deng, P.; Sei, E.; Maeda, D. Y.; Zebala, J. A.; Spring, D. J.; Kim, M.; Wang, H.; Maitra, A.; Moore, D.; Clise-Dwyer, K.; Wang, Y. A.; Navin, N. E.; DePinho, R. A. Targeting T cell checkpoints 41BB and LAG3 and myeloid cell CXCR1/CXCR2 results in antitumor immunity and durable response in pancreatic cancer. *Nat. Cancer.* **2023**, *4*, 62−80.
(36) Kumar, A.; Duffieux, F.; Gagnaire, M.; Rapisarda, C.; Bertrand, T.; Rak, A. Structural insights into epitope-paratope interactions of a monoclonal antibody targeting CEACAM5-expressing tumors. *Nat. Commun.* **2024**, *15*, No. 9377.
(37) Powell, E.; Shao, J.; Picon, H. M.; Bristow, C.; Ge, Z.; Peoples, M.; Robinson, F.; Jeter-Jones, S. L.; Schlosberg, C.; Grzeskowiak, C. L.; Yang, F.; Wu, Y.; Wistuba, I.; Moulder, S. L.; Symmans, W. F.; Scott, K. L.; Edwards, J. R.; Liang, H.; Heffernan, T. P.; Piwnica-Worms, H. A functional genomic screen in vivo identifies CEACAM5 as a clinically relevant driver of breast cancer metastasis. *npj Breast Cancer* **2018**, *4*, No. 9, DOI: 10.1038/s41523-018-0062-x.
(38) Galmiche, A.; Sauzay, C.; Houessinon, A.; Chauffert, B.; Pluquet, O. Probing Tumour Proteostasis and the UPR with Serum Markers. *Trends Cancer.* **2016**, *2*, 219−221.
(39) Qin, J.; Zhou, Y. J.; Krivoruchko, A.; Huang, M.; Liu, L.; Khoomrung, S.; Siewers, V.; Jiang, B.; Nielsen, J. Modular pathway rewiring of Saccharomyces cerevisiae enables high-level production of L-ornithine. *Nat. Commun.* **2015**, *6*, No. 8224, DOI: 10.1038/ncomms9224.
(40) Canè, S.; Geiger, R.; Bronte, V. The roles of arginases and arginine in immunity. *Nat. Rev. Immunol* **2025**, *25*, 266−284.
(41) Zhou, J.; Sun, X.; Jiang, P. The emerging roles of the urea cycle in tumor microenvironment and therapies. *Trends Cancer* **2025**, *11* (12), 1203−1209, DOI: 10.1016/j.trecan.2025.08.007.
(42) Lercher, A.; Bhattacharya, A.; Popa, A. M.; Caldera, M.; Schlapansky, M. F.; Baazim, H.; Agerer, B.; Gürtl, B.; Kosack, L.; Májek, P.; Brunner, J. S.; Vitko, D.; Pinter, T.; Genger, J.; Orlova, A.; Pikor, N.; Reil, D.; Ozsvár-Kozma, M.; Kalinke, U.; Ludewig, B.; Moriggl, R.; Bennett, K. L.; Menche, J.; Cheng, P. N.; Schabbauer, G.; Trauner, M.; Klavins, K.; Bergthaler, A. Type I Interferon Signaling Disrupts the Hepatic Urea Cycle and Alters Systemic Metabolism to Suppress T Cell Function. *Immunity* **2019**, *51*, 1074−1087.
(43) Spinelli, J. B.; Haigis, M. C. The multifaceted contributions of mitochondria to cellular metabolism. *Nat. Cell Biol.* **2018**, *20*, 745−754.
(44) Watson, C. T.; Cohain, A. T.; Griffin, R. S.; Chun, Y.; Grishin, A.; Hacyznska, H.; Hoffman, G. E.; Beckmann, N. D.; Shah, H.; Dawson, P.; Henning, A.; Wood, R.; Burks, A. W.; Jones, S. M.; Leung, D. Y. M.; Sicherer, S.; Sampson, H. A.; Sharp, A. J.; Schadt, E. E.; Bunyavanich, S. Integrative transcriptomic analysis reveals key drivers of acute peanut allergic reactions. *Nat. Commun.* **2017**, *8*, No. 1943.
(45) Pan, H.; Jiang, Y.; Boi, M.; Tabbò, F.; Redmond, D.; Nie, K.; Ladetto, M.; Chiappella, A.; Cerchietti, L.; Shaknovich, R.; Melnick, A. M.; Inghirami, G. G.; Tam, W.; Elemento, O. Epigenomic evolution in diffuse large B-cell lymphomas. *Nat. Commun.* **2015**, *6*, No. 6921, DOI: 10.1038/ncomms7921.
(46) Adam, R.; Spier, I.; Zhao, B.; Kloth, M.; Marquez, J.; Hinrichsen, I.; Kirfel, J.; Tafazzoli, A.; Horpaopan, S.; Uhlhaas, S.; Stienen, D.; Friedrichs, N.; Altmüller, J.; Laner, A.; Holzapfel, S.; Peters, S.; Kayser, K.; Thiele, H.; Holinski-Feder, E.; Marra, G.; Kristiansen, G.; Nöthen, M. M.; Büttner, R.; Möslein, G.; Betz, R. C.; Brieger, A.; Lifton, R. P.; Aretz, S. Exome Sequencing Identifies Biallelic MSH3 Germline Mutations as a Recessive Subtype of Colorectal Adenomatous Polyposis. *Am. J. Hum. Genet.* **2016**, *99*, 337−351.
(47) Yang, M.; Liu, Y.; Dai, J.; Li, L.; Ding, X.; Xu, Z.; Mori, M.; Miyahara, H.; Sawashita, J.; Higuchi, K. Apolipoprotein A-II induces acute-phase response associated AA amyloidosis in mice through conformational changes of plasma lipoprotein structure. *Sci. Rep.* **2018**, *8*, No. 5620, DOI: 10.1038/s41598-018-23755-y.
(48) Chen, M.-M.; Gao, Q.; Ning, H.; Chen, K.; Gao, Y.; Yu, M.; Liu, C.; Zhou, W.; Pan, J.; Wei, L.; Dou, W.; Zhang, D.; Zhu, L.; Zhang, Q.; Chen, R.; Zhang, Z. Integrated single-cell and spatial transcriptomics uncover distinct cellular subtypes involved in neural invasion in pancreatic cancer. *Cancer Cell* **2025**, *43*, 1656−1676.

https://doi.org/10.1021/acs.analchem.5c08111
Anal. Chem. 2026, 98, 11261−11273

(49) Rakina, M.; Larionova, I.; Kzhyshkowska, J. Macrophage diversity in human cancers: New insight provided by single-cell resolution and spatial context. *Heliyon* **2024**, *10*, No. e28332, DOI: 10.1016/j.heliyon.2024.e28332.
(50) Zhou, Y.; Shen, G.; Zhou, X.; Li, J. Therapeutic potential of tumor-associated neutrophils: dual role and phenotypic plasticity. *Signal Transduction Targeted Ther.* **2025**, *10*, No. 178, DOI: 10.1038/s41392-025-02242-7.
(51) Niu, L.; Gao, C.; Li, Y. Identification of potential core genes in colorectal carcinoma and key genes in colorectal cancer liver metastasis using bioinformatics analysis. *Sci. Rep.* **2021**, *11*, No. 23938, DOI: 10.1038/s41598-021-03395-5.
(52) Li, Y.-l.; Wu, L.; Zeng, L.; Zhang, Z.; Wang, W.; Zhang, C.; Lin, N. ApoC1 promotes the metastasis of clear cell renal cell carcinoma via activation of STAT3. *Oncogene* **2020**, *39*, 6203−6217.
(53) Caronni, N.; La Terza, F.; Vittoria, F. M.; Barbiera, G.; Mezzanzanica, L.; Cuzzola, V.; Barresi, S.; Pellegatta, M.; Canevazzi, P.; Dunsmore, G.; Leonardi, C.; Montaldo, E.; Lusito, E.; Dugnani, E.; Citro, A.; Ng, M. S. F.; Schiavo Lena, M.; Drago, D.; Andolfo, A.; Brugiapaglia, S.; Scagliotti, A.; Mortellaro, A.; Corbo, V.; Liu, Z.; Mondino, A.; Dellabona, P.; Piemonti, L.; Taveggia, C.; Doglioni, C.; Cappello, P.; Novelli, F.; Iannacone, M.; Ng, L. G.; Ginhoux, F.; Crippa, S.; Falconi, M.; Bonini, C.; Naldini, L.; Genua, M.; Ostuni, R. IL-1β+ macrophages fuel pathogenic inflammation in pancreatic cancer. *Nature* **2023**, *623*, 415−422.
(54) Subramanian, S. P.; Gundry, R. L. The known unknowns of apolipoprotein glycosylation in health and disease. *iScience* **2022**, *25*, No. 105031.
(55) Cochran, B. J.; King, T. W.; Chemello, K.; Thomas, S. R.; Rye, K. HDL metabolism and function in diabetes mellitus. *Nat. Rev. Endocrinol* **2025**, *22*, 36−49, DOI: 10.1038/s41574-025-01176-y.
(56) Shi, X.; Feng, D.; Li, D.; Han, P.; Yang, L.; Wei, W. A pan-cancer analysis of the oncogenic and immunological roles of apolipoprotein F (APOF) in human cancer. *Eur. J. Med. Res.* **2023**, *28*, No. 190, DOI: 10.1186/s40001-023-01156-w.
(57) Lecordier, L.; Heo, P.; Graversen, J. H.; Hennig, D.; Skytthe, M. K.; Cornet D'elzius, A.; Pincet, F.; Pérez-Morga, D.; Pays, E. Apolipoproteins L1 and L3 control mitochondrial membrane dynamics. *Cell Rep.* **2023**, *42* (12), No. 113528.
(58) Ding, Z.; Wu, J.; Ye, Y.; Zhong, Y.; Yan, L.; Wang, P. A novel signature predicts prognosis in pancreatic cancer based on tumor membrane-associated genes. *Heliyon* **2025**, *11* (4), No. e42791, DOI: 10.1016/j.heliyon.2025.e42791.
(59) Beckerman, P.; Bi-Karchin, J.; Park, A. S. D.; Qiu, C.; Dummer, P. D.; Soomro, I.; Boustany-Kari, C. M.; Pullen, S. S.; Miner, J. H.; Hu, C. A.; Rohacs, T.; Inoue, K.; Ishibe, S.; Saleem, M. A.; Palmer, M. B.; Cuervo, A. M.; Kopp, J. B.; Susztak, K. Transgenic expression of human APOL1 risk variants in podocytes induces kidney disease in mice. *Nat. Med.* **2017**, *23*, 429−438.
(60) Zhu, J.; Zhao, J.; Luo, C.; Zhu, Z.; Peng, X.; Zhu, X.; Lin, K.; Bu, F.; Zhang, W.; Li, Q.; Wang, K.; Hu, Z.; Yu, X.; Chen, L.; Yuan, R. FAT10 promotes chemotherapeutic resistance in pancreatic cancer by inducing epithelial-mesenchymal transition via stabilization of FOXM1 expression. *Cell Death Dis.* **2022**, *13*, No. 497, DOI: 10.1038/s41419-022-04960-0.
(61) Xie, Y.; Zhu, S.; Song, X.; Sun, X.; Fan, Y.; Liu, J.; Zhong, M.; Yuan, H.; Zhang, L.; Billiar, T. R.; Lotze, M. T.; Zeh, H. J.; Kang, R.; Kroemer, G.; Tang, D. The Tumor Suppressor p53 Limits Ferroptosis by Blocking DPP4 Activity. *Cell Reports* **2017**, *20*, 1692−1704.
(62) Obradovic, K. S.; Ebner, F.; Artemov, A. V.; Miotto, M.; Traexler, P.; Jacob, R.; Thanh, H. P. T.; Ruzicka, R.; Wernitznig, A.; Baumann, I.; Gerlach, D.; Impagnatiello, M.; Siena, S.; Murphy, M.; House, R.; Reiser, U.; Santoro, V.; Popow, J.; Carotta, S.; Baum, A.; Lipp, J.; Bardelli, A.; Tontsch-Grunt, U.; Russo, M.; Aichinger, M. Combining BET inhibition with SMAC mimetics restricts tumor growth and triggers immune surveillance in preclinical cancer models. *Cell Rep. Med.* **2025**, *6*, No. 102313, DOI: 10.1016/j.xcrm.2025.102313.
(63) Li, W.; Yao, C.; Guo, H.; Ni, X.; Zhu, R.; Wang, Y.; Yu, B.; Feng, X.; Gu, Z.; Da, Z. Macrophages communicate with mesangial cells through the CXCL12/DPP4 axis in lupus nephritis pathogenesis. *Cell Death Dis.* **2024**, *15* (5), No. 344, DOI: 10.1038/s41419-024-06708-4.
(64) De Jaeghere, E. A.; Denys, H. G.; De Wever, O. Fibroblasts Fuel Immune Escape in the Tumor Microenvironment. *Trends Cancer* **2019**, *5*, 704−723.
(65) Wang, Y.; Sun, Z.; Ping, J.; Tang, J.; He, B.; Chang, T.; Zhou, Q.; Yuan, S.; Tang, Z.; Li, X.; Lu, Y.; He, R.; He, X.; Liu, Z.; Yin, L.; Wu, N. Cell volume controlled by LRRC8A-formed volume-regulated anion channels fine-tunes T cell activation and function. *Nat. Commun.* **2023**, *14*, No. 7075, DOI: 10.1038/s41467-023-42817-y.
(66) Llorente, A.; Arora, G. K.; Murad, R.; Emerling, B. M. Phosphoinositide kinases in cancer: from molecular mechanisms to therapeutic opportunities. *Nat. Rev. Cancer* **2025**, *25*, 463−487.
(67) He, M.; Liu, Y.; Chen, S.; Deng, H.; Feng, C.; Qiao, S.; Chen, Q.; Hu, Y.; Chen, H.; Wang, X.; Jiang, X.; Xia, X.; Zhao, M.; Lyu, N. Serum amyloid A promotes glycolysis of neutrophils during PD-1 blockade resistance in hepatocellular carcinoma. *Nat. Commun.* **2024**, *15*, No. 1754, DOI: 10.1038/s41467-024-46118-w.
(68) Lee, J.-Y.; Hall, J. A.; Kroehling, L.; Wu, L.; Najar, T.; Nguyen, H. H.; Lin, W.; Yeung, S. T.; Silva, H. M.; Li, D.; Hine, A.; Loke, P.; Hudesman, D.; Martin, J. C.; Kenigsberg, E.; Merad, M.; Khanna, K. M.; Littman, D. R. Serum Amyloid A Proteins Induce Pathogenic Th17 Cells and Promote Inflammatory Disease. *Cell* **2020**, *180*, 79−91.
(69) Pereira, B. A.; Vennin, C.; Papanicolaou, M.; Chambers, C. R.; Herrmann, D.; Morton, J. P.; Cox, T. R.; Timpson, P. CAF Subpopulations: A New Reservoir of Stromal Targets in Pancreatic Cancer. *Trends Cancer* **2019**, *5*, 724−741.
(70) Wu, J.-L.; Su, T.; Chen, P.; Chen, Y. Acute-phase serum amyloid A for early detection of hepatocellular carcinoma in cirrhotic patients with low AFP level. *Sci. Rep* **2022**, *12*, No. 5799, DOI: 10.1038/s41598-022-09713-9.